ISSN 1330-3651 (Print), ISSN 1848-6339 (Online) https://doi.org/10.17559/TV-20230809000866
Original scientific paper

Optimal Differential Control for Accurate Positioning of Medical Electronic Wristband

Wei LI*, Xeu-qin MENG, Chang-song MA

Abstract: In this paper, an improved differential evolution algorithm is proposed to improve the positioning accuracy of electronic wristband system. The wristband system is composed of STM32F103 microcontroller, Beidou positioning module, LORA communication module and so on. In the traditional differential evolution algorithm, premature convergence to local optimal will reduce the accuracy of the algorithm. To solve this problem, the method introduces the distance information between known and unknown points and between all unknown points in the fitness function and overall initialization. This reduces the premature convergence of the algorithm and improves the optimization ability of the algorithm. Experimental results using the CICDDoS2019 dataset show that the localization accuracy of the proposed algorithm is improved by 7.6% compared with traditional differential evolution. The method also has good stability. This provides an effective way to improve the positioning accuracy of the wristband, which can be used for applications such as patient monitoring.

Keywords: convergence; differential evolution algorithm; electronic wristbands; fitness function; LORA communication

1 INTRODUCTION

Medical wristband, also known as medical identification band, is a carrier for hospitals to record information of patients (inpatients). It is characterized by one-time, one-to-one, independent, accurate and convenient recording of patients' personal information and case information, etc. Its function is to ensure "five correct" in the treatment process of patients [1-3]. The medical electronic wristband also has real-time positioning function to realize the digital care of hospitalized patients. Electronic wristbands have become an important technology for applications such as patient monitoring and fitness tracking. One of the key functions provided by this wristband is positioning, precisely locating and tracking the position of the wearer. However, due to the limitation of the positioning algorithm, the positioning accuracy of the existing wristband system is not ideal. This hinders their effectiveness in critical applications. A variety of techniques have been explored to enhance wristband positioning, including genetic algorithm [4], differential evolution algorithm [5], particle swarm algorithm [6], slope climbing algorithm [7], neural network algorithm [8], sparrow algorithm [9], and chicken cooperative positioning algorithm [10].

In literature [11], genetic algorithm is adopted. In the process of solving positioning, the search starts from string set, which has a large coverage and is conducive to global search, and the output results can be obtained quickly with good real-time performance. In literature [12], differential evolution algorithm was adopted to reduce positioning errors and achieve accurate positioning. Literature [13] adopts an adaptive particle swarm positioning algorithm, which adaptively adjusts the cross probability and variation factors of each generation to better search the global optimal location. Literature [14] adopts a hybrid algorithm based on the climbing method and heuristic, and uses a new crossover process to generate a new generation of individuals. Literature [15] and [16] adopted a hybrid positioning algorithm based on neural network algorithm and Taylor series expansion. The optimal value obtained by the neural network algorithm was taken as the initial value, and the Taylor series iterative algorithm was used for local optimization to obtain the precise location of nodes. Among them, differential evolution algorithm is a powerful optimization algorithm, which has the characteristics of simple structure, high optimization efficiency, low code density and good convergence, etc., and has been widely used [17-20]. However, in the process of solving the algorithm, with the increase of evolutionary algebra, the diversity of the population will become smaller, premature convergence to the local minimum point, resulting in stagnation of the algorithm, and the performance of the algorithm deteriorates in the process of evolution. Among them, differential evolution has become a popular method because of its simple structure, fast convergence and global search ability. However, the traditional differential evolution algorithm has some problems such as premature convergence, which reduces the accuracy of the algorithm. To address these limitations, an improved differential evolution wristband location algorithm is proposed in this paper. The main contribution is to introduce inter-point distance information into fitness evaluation and population initialization to reduce premature convergence and improve optimization ability. This is for quality monitoring applications to improve the accuracy of wristband positioning.

2 IMPROVE DIFFERENTIAL EVOLUTION ALGORITHM DESIGN

2.1 Differential Evolution Localization Principle

In the design, the localization process is transformed into differential evolution algorithm. In the system of m known positioning coordinate points and n unknown positioning coordinate points, the distance between known point and unknown point is $d_{m\to n}$, and the distance between each unknown point is $\hat{d}_{n\to k}$. Let the coordinates of m known points be (a_k, b_k) , and the coordinates of n unknown points be (x_i, y_j) , where k is a positive integer.

$$\begin{cases} d_{1\to 1} = \sqrt{(x_1 - a_1)^2 - (y_1 - b_1)^2} + \sigma_{1\to 1} \\ ..... \\ d_{m\to n} = \sqrt{(x_m - a_n)^2 - (y_m - b_n)^2} + \sigma_{m\to n} \end{cases}$$

$$\hat{d}_{i\to j}=\sqrt{\left(x_i-x_j\right)^2-\left(y_i-y_j\right)^2}+\sigma_{i\to j} \tag{1}$$

where, $\sigma_{i\to j}$ is the measurement error.

The flow of differential evolution algorithm is shown in Fig. 1 below:

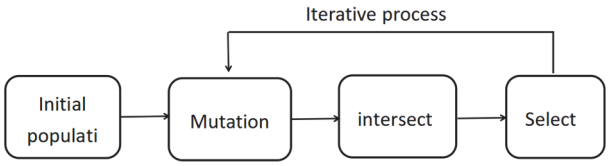

Figure 1 Differential evolution algorithm flow

2.2 Improved Differential Evolution Algorithm Design

Differential evolution algorithm is an efficient global optimization algorithm, which is implemented by heuristic search method based on population [21, 22]. The implementation steps are as follows: random generation of initial population → construction of fitness function → mutation operation → crossover operation → selection operation.

1. Randomly generate the initial population. Assume that the population with dimension 2 and size M is randomly initialized, and the population is randomly initialized as follows:

$$X_M^0=\text{rand}(0,1)\times(X_M^H-X_M^L)+X_M^H \tag{2}$$

where, $\text{rand}(0,1)$ is a random number between 0 and 1, and X_M^H, X_M^L is the largest, smallest and smallest value of a one-dimensional parameter of dimension.

2. Construct fitness function. Fitness function is used to evaluate the merits and demerits of individuals, and the iteration range of the algorithm can be effectively enhanced through fitness function [23-25]. Let the M-th individual of the NTH generation be: $X_M^N=\left(x_{i\to M}^N, y_{i\to M}^N\right)$. The fitness function of differential evolution algorithm can be expressed as:

$$f\left(X_M^N\right)=\frac{1}{K}\sum_{K=1}^{K}\left(\sqrt{(x_{i\to M}^N-a_K)^2+(y_{i\to M}^N-b_K)^2}-d_{i\to K}\right)^2 \tag{3}$$

1. Mutation operation. The application function of differential variation strategy can obtain the variation individual after variation operation, which can be expressed as:

2.

$$W_M^N=X_{r1}^N+L\times\left(X_{r2}^N-X_{r3}^N\right) \tag{4}$$

r_1, r_2, r_3 is a random number; L is the scaling factor, which controls the variation step size and ranges from 0 to 1. $X_{r2}^N-X_{r3}^N$ is the difference.

According to Eq. (4), the mutant individuals can be obtained as follows:

$$W_M^N=\left(w_{i\to M}^N(x)-w_{i\to M}^N(y)\right) \tag{5}$$

4. Cross operation. The mutated individual is compared with the corresponding individual in the contemporary population. It can be expressed as:

$$v_M^N=\begin{cases}W_M^N, r_i<P_{r_i};\\ X_M^N, \text{otherwise};\end{cases} \tag{6}$$

In the command, r_i is a random number ranging from 0 to 1. P_{r_i} is the crossover probability.

Cross individuals are obtained:

$$V_M^N=\left\{v_{1\to M}^N(x), v_{1\to M}^N(y), \cdots v_{i\to M}^N(x), v_{i\to M}^N(y)\right\} \tag{7}$$

5. Select an operation. If the fitness of the mutated individual is better than that of the current individual, the old individual will be replaced by the mutated individual in the next generation, otherwise the old individual will still be preserved.

Specifically, the fitness function values of the current individual and the cross individual are compared by Eq. (3), so as to select the individuals entering the next generation. The expression is as follows:

$$X_M^{N+1}=\begin{cases}X_M^N, \text{if}(f(X_M^N)\le f(V_M^N))\\ V_M^N, \text{otherwise}\end{cases} \tag{8}$$

In this evolutionary process, the impact of ranging error on positioning accuracy can be effectively reduced, but the evolutionary process did not consider the distance value $\hat{d}_{n\to k}$ between unknown anchor points, so a method is proposed to improve the fitness function and add the distance information between unknown anchor points in Eq. (3), so as to ensure that the $\hat{d}_{n\to k}$ value is fully used in the positioning calculation process. The implementation process is shown in Fig. 2.

In Fig. 2, the improved fitness function is expressed as follows:

$$\begin{aligned}f(X_M^N)=U_1\sum_{i=1}^{n}\sum_{K=1}^{m}\left(\sqrt{\left(x_{i\to M}^N-a_K\right)^2+\left(y_{i\to M}^N-b_K\right)^2}-d_{m\to n}\right)^2\\ +U_2\sum_{i=1}^{n-1}\sum_{j=1}^{m}\left(\sqrt{\left(x_{i\to M}^N-x_{j\to M}^N\right)^2+\left(y_{i\to M}^N-y_{j\to M}^N\right)^2}-\hat{d}_{i\to j}\right)^2\end{aligned} \tag{9}$$

where, U_1, U_2 is the calculation coefficient. $\left\{X_1^N, X_2^N, \cdots, X_M^N\right\}$ is the initialization coordinate array constructed by m known and n unknown positioning coordinate points.

$\left\{x_{1\to \mathrm{M}}^N, y_{1\to \mathrm{M}}^N, x_{2\to M}^N, y_{2\to \mathrm{M}}^N, \cdots, x_{i\to M}^N, y_{i\to \mathrm{M}}^N\right\}$ is the successful individual in the iterative process.

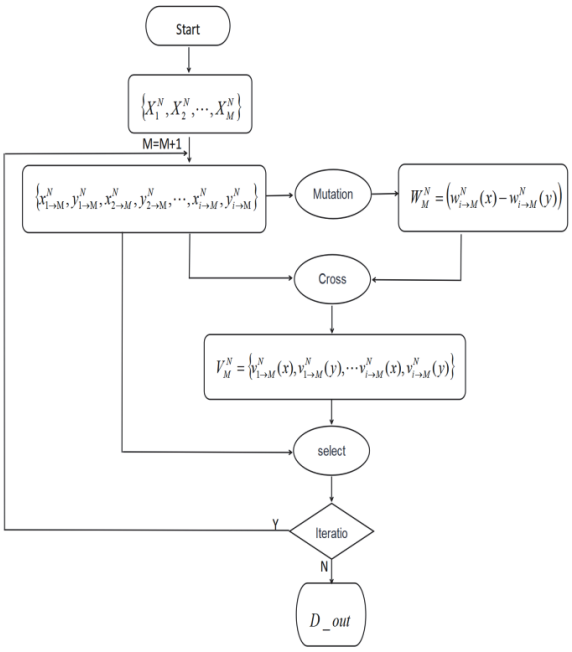

Figure 2 Block diagram of improved differential evolution algorithm

where, D_out is the output of the improved difference carry algorithm, which is not only related to known measuring point coordinates, but also to unknown measuring point coordinates. By introducing the unknown measuring point coordinate distance value into the algorithm, the controllability of the whole algorithm to the unknown coordinate distance value is enhanced, the stability is enhanced, and the precision of the output value of the whole system is improved, independent of the system environment, which greatly enhances the control accuracy of the system. The software implementation logic of improved differential carry algorithm is shown in Fig. 3.

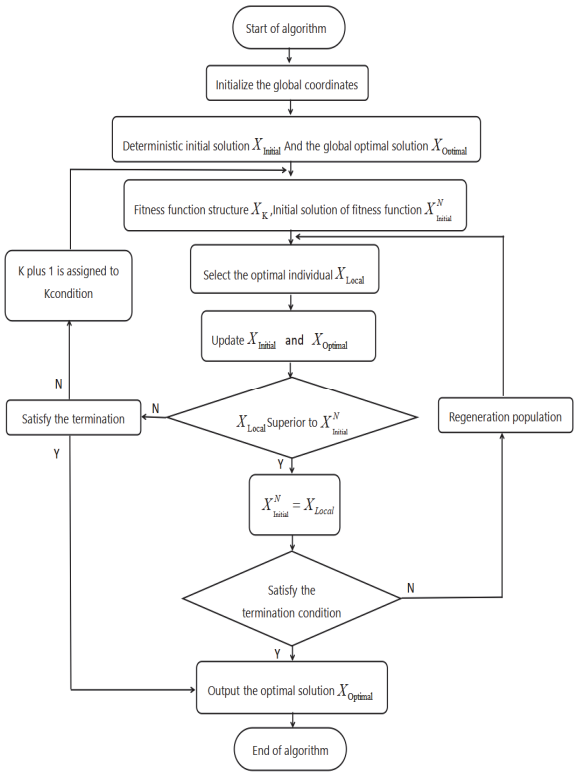

Figure 3 Flow chart of software implementation of improved differential evolution algorithm

The Matlab test program is as follows:

```
Function_name='F1';
    [lb,ub,dim,fobj]=Get_Functions_details(Function_name);
    size = 50;
    iter_max = 1000;
  range_max_list = ones(1, dim)*ub;
  range_min_list = ones(1, dim)*lb;
base=DE_Impl(dim,size,iter_max,range_min_list,range_max_lis
t);
base.is_cal_max = false;
base.fitfunction =fobj;
base.run();
```

3 CONSTRUCTION OF ACCURATE POSITIONING SYSTEM FOR ELECTRONIC WRISTBAND

The positioning system of an electronic wristband consists of an electronic wristband, a wireless gateway, a background server, a personal computer, and a mobile device (APP). See Fig. 4.

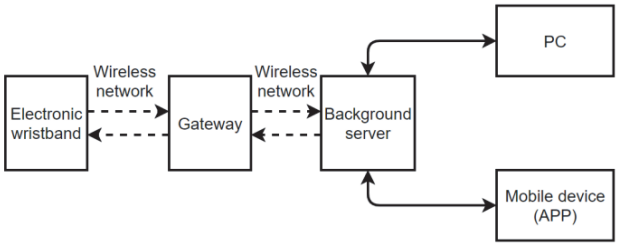

Figure 4 Electronic wrist band management system

The electronic wristband is composed of STM32F103RBT6 as the core controller, positioning module, LORA communication module, man-machine interface and system power supply. The block diagram is shown in Fig. 5. In the implementation, a high precision positioning system based on the improved differential evolution algorithm is constructed.

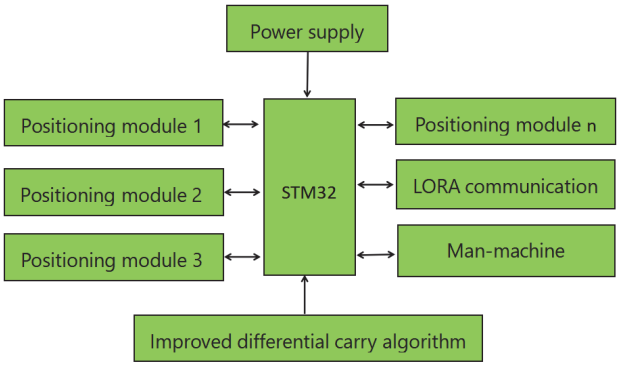

Figure 5 Block diagram of medical electronic wristband

After the system is started, the retained coordinate data information is first queried in the flash memory integrated inside the STM32F103RBT6 chip. If there is no data, the data stored on the gateway can be automatically obtained into the flash memory through the LORA gateway. After receiving the command, the positioning module sends its own coordinate data to the master controller every 150ms. The master controller transmits the received coordinate data information to the improved differential carry algorithm to calculate the coordinates of unknown measuring points.

a) Main Control Circuit

The microcontroller adopts STM32F103RBT6, encapsulates LQFP48, has a length and width of 7 mm, and has three serial ports [26]. In the design, serial port 1 communicates with LORA module and serial port 2 is used as debugging serial port to print information. The circuit is shown in Fig. 6. Power pin 3V3 is externally connected with 3.3 V input DC voltage; Y1 is an 8MHz passive crystal oscillator, which, together with C39 and C40, forms the external system clock circuit. R51 and C43 are external power-on reset circuits; Interface P2 is the reserved debugging serial port, where UART2_RX is the data receiving pin and UART2_TX is the data sending pin. Interface P3 is the burning port of ST_LINK program. R3 is a pull-down resistor that enables the program to burn to an internal FLASH address.

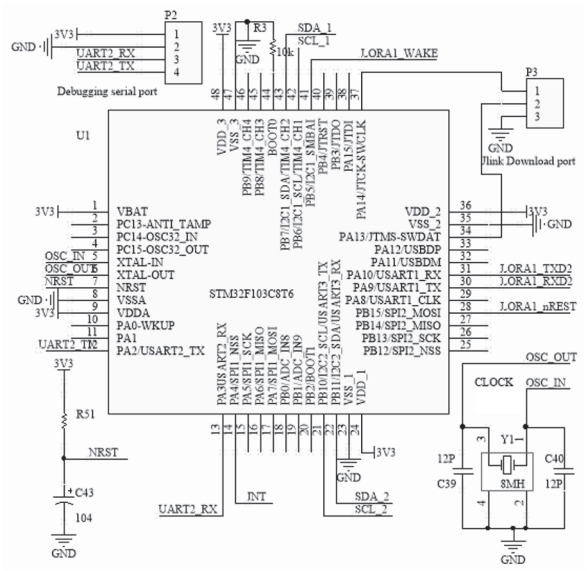

Figure 6 Main control circuit

b) LORA Module Circuit

LORA module model Ra-01 (SX1278 chip) has an effective transmission distance of 10 Km, transmission power consumption of 93 mA, and 1.6 mA in sleep mode [27]. The WAKE pin of the LORA module is connected to the IO port of the STM32. When the LORA module enters the low power mode, it can wake up by dropping edge level through the pin. The module circuit is shown in Fig. 7. PIN13 and PIN14 of LORA module are power supply pins, which are connected to 3.3V DC voltage for power supply. Capacitor C1 is an energy storage capacitor of 100uF, which provides large current at the moment of module startup. PIN1 and PIN3 are grounded, and PIN2 is Π impedance matching network composed of inductors L1, capacitors C3 and C4. L1 parameter is ±1%, and inductance value 4.7 nH. The accuracy of C3 and C4 was ±1%, and the volume value was 1.2 pF. Antenna Access ESD Protection Diode, Model SESD3Z08C; The LORA module antenna uses 50 Ω impedance matching. In the actual circuit board design, the PCB board thickness is 1 mm, the RF antenna line width is 36.614 mil (1 mil = 0.0254 mm), and the route is as short as possible, covering the ground. The LORA module is implemented with an active antenna. PIN19 and PIN20 are the serial communication pins of the module, which are directly connected to the serial port 1 pin of STM32 to realize communication data interaction. PIN4 is the reset pin of the module, and external NPN type triode Q2, model 8050, triode Q2 and R5 form a logic non-circuit, and then the reset signal sent by STM32 controls the reset state of LORA module. Resistors R4 and R6 are pull-up resistors to keep the module working in the initial mode.

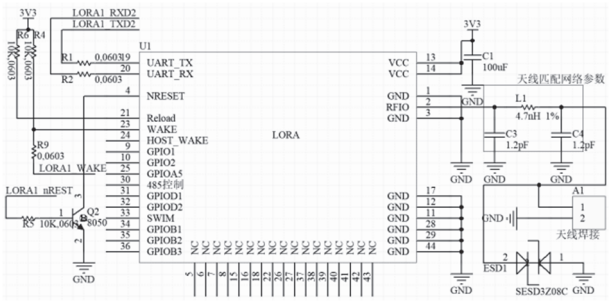

Figure 7 Lora circuit

c) Locating Module Circuits

The location module model is SIM868. SIM868 module is a four-band GSM/GPRS module integrating GPS/GLONASS/BDS (GPS/GLONASS/BDS) technology [28]. The circuit is shown in Fig. 8. A1 is passive GPS antenna; C65, C66 and R63 form Π impedance matching network; power supply voltage range is 3.4 V - 4.4 V. When transmitting signals, the maximum power of the power supply is greater than 2A; C4 is the ESR bypass capacitor of the VBAT pin. The value is 220 uF and is as close to the module pin as possible. The antenna of SIM868 module uses 50 Ω impedance matching. In the actual circuit board design, the PCB board thickness is 1 mm, the RF antenna line width is 36.614 mil (1 mil = 0.0254 mm), and the routes are as short as possible, covering the ground.

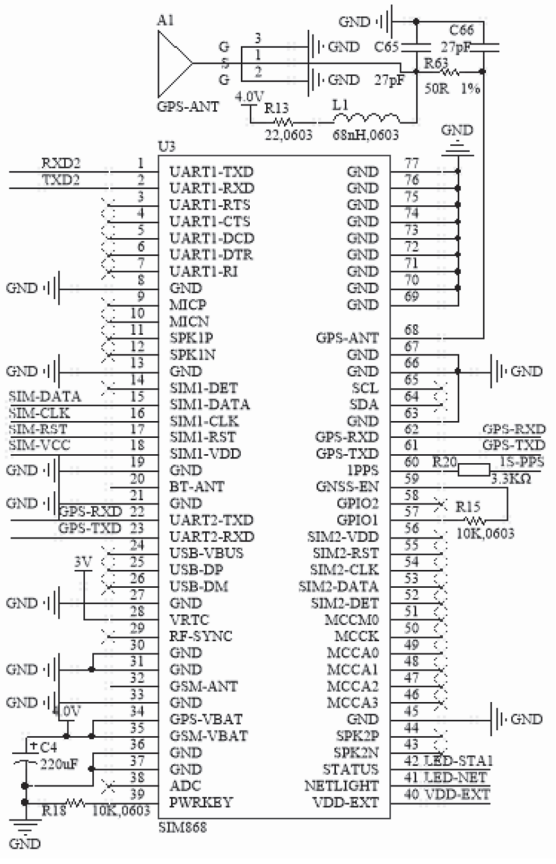

Figure 8 Positioning module circuit

d) Power Circuit

The wrist strap provides external power supply and built-in battery power supply, which can be switched through the circuit shown in Fig. 9. When port P10 is connected to the external power, the current passes through the resistor R51 and R52, divides the voltage on R52 and then connects to the grid of field effect tube Q18. The field effect tube Q18 has drain-source cut-off, and the battery BAT-V3.3 cannot supply power to the device circuit. At the same time, the input current passes through diode D2 to supply 3.3 V to the device (3V3 in Fig. 7). When the external power is removed, the grid potential of the field effect tube Q18 is pulled down to zero potential by the resistor R52. Q18 is drain-source switched on, and the battery provides 3.3 V voltage to the device circuit. Meanwhile, P10 no longer has voltage under D2 single pass characteristics.

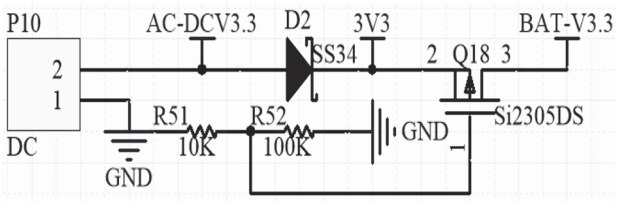

Figure 9 Power switching circuit

e) Man-Machine Interface

Man-machine interface mainly refers to the key input module and display output module. Key input is realized by an independent key. Press the key for 3 s to start the machine, and press the key for 10s to enter the mode setting. The display is 0.96 "blue light OLED.

4 SYSTEM SOFTWARE DESIGN

The system software design idea is shown in Fig. 10.

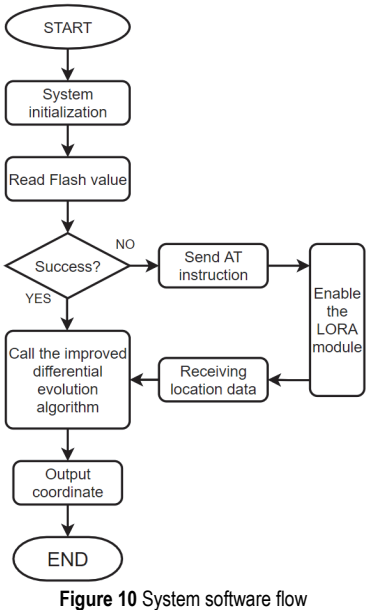

Figure 10 System software flow

After the system is running, the first step is to initialize each module, including: SCM clock configuration, interrupt vector nesting configuration, GPIO configuration, serial communication configuration, Flash read-write configuration, LORA module initialization, positioning module initialization, differential evolution algorithm initialization. The second step reads the Flash stored value, and receives the positioning data transmitted by the positioning module according to the 150 ms sampling period. The third step calls LORA communication module through AT instruction, establishes data communication with gateway, transmits or receives positioning data. The fourth step is to transfer the distance values between known points and unknown points and the distance values between unknown points to the improved difference carry algorithm to calculate the coordinates of unknown anchor points. In the design, the receiving and positioning module data adopts the periodic receiving mode, and uses timer 5 to set the receiving rate.

The optimization program is implemented as follows:

```
classdef Algorithm_Impl &lt;
function init(self)
self.position_best=zeros(1,self.dim);
self.value_best_history=[];
self.position_best_history=[];
self.value_best = -realmax('double');
end
function iteration(self)
for iter = 1:self.iter_max
self.update(iter)
end
function update(self,iter)
for i = 1:self.size
if(self.unit_list(i).value&gt; self.value_best)
self.value_best = self.unit_list(i).value;
self.position_best = self.unit_list(i).position;
end
if(self.is_cal_max)
self.value_best_history(end+1) = self.value_best;
else
self.value_best_history(end+1) = -self.value_best;
end
self.position_best_history=
[self.position_best_history;self.position_best];
disp([' optimal solution =' num2str(self.position_best)]);
end
function value = cal_fitfunction(self,position)
if(isempty(self.fitfunction))
value = 0;
else
if(self.is_cal_max)
value = self.fitfunction(position);
else
value = -self.fitfunction(position);
end
self.cal_fit_num = self.cal_fit_num+1;
end
function s=get_out_bound_value(self,position,min_list,max_list)
if(~exist('min_list','var'))
min_list = self.range_min_list;
end
if(~exist('max_list','var'))
max_list = self.range_max_list;
end
position_tmp=position;
I=position_tmp&lt; min_list;
position_tmp(I)=min_list(I);
J=position_tmp&gt; max_list;
position_tmp(J)=max_list(J);
s=position_tmp;
end
position_rand= unifrnd(self.range_min_list,self.range_max_list);
```

```
position_tmp=position;
I=position_tmp&lt; min_list;
position_tmp(I)=position_rand(I);
J=position_tmp&gt; max_list;
position_tmp(J)=position_rand(J);
s=position_tmp;
end
```

5 ALGORITHM TESE

In order to improve the reliability of the algorithm, MATLAB simulation is used to verify the performance of relevant parameters, so as to verify the actual performance of the improved differential carry algorithm [29, 30]. In the simulation test, the population (number of coordinate points) scale was set to $M = 30$, and the maximum number of iterations was set to $N = 100$, $N = 300$, and $N = 600$ respectively. $L = 0.7$, $r_i = 0.28$.

In the matlab command window, type:

>>[xm, fv] = DE (@ fitness, 30, 0.7, 0.28, 100, 30)

>>[xm, fv] = DE (@ fitness, 30, 0.7, 0.28, 300, 30)

>>[xm, fv] = DE (@ fitness, 30, 0.7, 0.28, 600, 30)

The following data list is obtained:

Table 1 Changes in iterative convergence data

M	100	300	600
*x*1	0	–1.29E–02	1.78E–04
*x*2	0	–4.13E–02	–1.17E–04
*x*3	0	9.91E–03	5.85E–05
*x*4	0	–2.09E–02	7.21E–05
*x*5	0	6.25E–03	–1.59E–04
*x*6	0	8.33E–03	9.52E–05
*x*7	0	–1.78E–02	–3.01E–04
*x*8	0	–5.52E–03	–2.26E–04
*x*9	0	9.74E–03	4.80E–05
*x*10	0	3.02E–02	–4.12E–05
*x*11	0	–1.64E–02	1.00E–04
*x*12	0	8.56E–03	2.75E–05
*x*13	0	–6.15E–03	2.45E–05
*x*14	0	–3.49E–03	–1.35E–04
*x*15	0	4.24E–02	2.66E–05
*x*16	0	–5.84E–02	1.35E–04
*x*17	0	5.51E–02	–4.93E–O5
*x*18	0	–1.10E–02	2.51E–04
*x*19	0	1.47E–02	1.50E–04
*x*20	0	1.11E–02	–4.13E–05
*x*21	0	6.87E–02	8.12E–05
*x*22	0	–1.80E–02	–3.78E–05
*x*23	0	1.32E–03	–2.59E–04
*x*24	0	–2.25E–02	–9.06E–05
*x*25	0	2.47E–02	–6.93E–05
*x*26	0	–1.73E–03	2.36E–04
*x*27	0	2.95E–02	–2.37E–04
*x*28	0	2.49E–02	–7.77E–05
*x*29	0	–1.87E–02	–6.81E–05
*x*30	0	2.16E–02	1.31E–04

As can be seen from Tab. 1, after a certain number of iterations, the algorithm can be optimized to obtain good results and improve the accuracy of the results. It also converges faster. The convergence calculation time and convergence rate are shown in Tab. 2.

Table 2 Algorithm performance test

turn	I	II	III	IV
Calculation time / ms	15.1	15.1	15.1	15.1
Rate of convergence / %	3.251	3.248	3.247	3.249

As can be seen from Tab. 2, in multiple calculations, the calculation time is maintained at 15.1 ms and the convergence rate is maintained at 3.25%.

The positioning error of coordinate points can be calculated by the following formula [31]:

$$error = \frac{\sum_{i=1,j=1}^{N} \sqrt{(x_i - x_j)^2 + (y_i - y_j)^2}}{N} \tag{10}$$

The traditional difference carry algorithm and the improved difference carry algorithm are shown in Fig. 11. The calibration distance of the measuring point is 10 m.

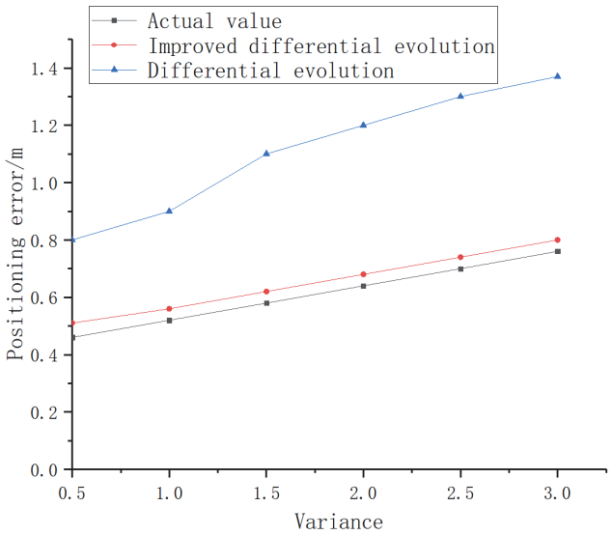

Figure 11 MATLAB simulation of improved differential evolution algorithm

The simulation results show that the location error decreases with the decrease of ranging error. For the same ranging error, the positioning error of the differential carry algorithm after adding the distance information between the unknown points is significantly lower than that of the algorithm without adding the distance information between the unknown points, and the algorithm performance is enhanced.

The calibration distance of the measuring point is 100 m, and the MATLAB simulation results are shown in Fig. 12.

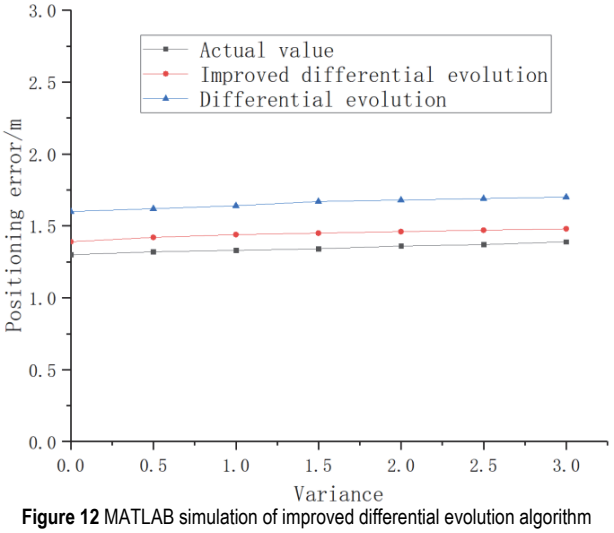

Figure 12 MATLAB simulation of improved differential evolution algorithm

The simulation results show that the improved differential carry algorithm has good stability in improving the positioning accuracy in large distance measurement.

Modeling simulation test was conducted on the improved differential evolution algorithm control system. It can be seen from the test results that the accuracy of positioning measurement is improved from 13.3% to 5.7%, and the accuracy is increased by 7.6%.

The above simulation results can be obtained by programming the algorithm modeling and installing it on the physical platform. The measurement results are shown in Table 3. It can be seen that the proposed algorithm has good stability and adaptability in measuring accuracy.

Table 3 Physical measurement results

Measured value	index	Difference algorithm	Differential carry algorithm	Textual algorithm
5 m	Relative error / %	> 0.50	> 0.38	< 0.27
	Standard deviation /m	> 2.50	> 2.00	< 1.20
10 m	Relative error / %	> 0.71	> 0.69	< 0.29
	Standard deviation / m	> 3.70	> 2.90	< 1.30
100 m	Relative error / %	> 0.87	> 0.89	< 0.30
	Standard deviation / m	> 5.70	> 3.90	< 1.37

6 CONCLUSION

In differential evolution algorithm, setting appropriate boundary conditions is helpful to improve the measurement accuracy of the algorithm. Based on this idea, in the traditional differential evolution algorithm, by introducing all the distance information between known points and unknown points and the distance information between unknown points into the fitness function and the initial population, the premature convergence of the algorithm is reduced, the optimization ability of the algorithm is enhanced, and the positioning measurement accuracy is improved. In the application of medical electronic wristband, the indoor positioning accuracy is effectively improved, and the safety of inpatients is ensured. Limitations of this study include the need to evaluate on more complex real-world datasets and benchmark against more localization algorithms. Future work could focus on implementing the method on physical wristband devices and investigating adaptive parametric tuning methods to further optimize accuracy.

Acknowledgment

Supported by Sichuan Science and Technology Program, China: 2023JDR0194.

7 REFERENCES

[1] Selder, J. L., Te Kolste, H. J., Twisk, J., Schijven, M., Gielen, W., & Allaart, C. P. (2023). Accuracy of a Standalone Atrial Fibrillation Detection Algorithm Added to a Popular Wristband and Smartwatch: Prospective Diagnostic Accuracy Study. *Journal of Medical Internet Research*, *25*, e44642. https://doi.org/10.2196/44642

[2] Mitro, N., Argyri, K., Pavlopoulos, L., Kosyvas, D., Karagiannidis, L., Kostovasili, M., ... & Amditis, A. (2023). AI-Enabled Smart Wristband Providing Real-Time Vital Signs and Stress Monitoring. *Sensors*, *23*(5), 2821. https://doi.org/10.3390/s23052821

[3] Ejaz, A., Jabeen, I., Khan, Z. U., Alomainy, A., Aljaloud, K., Alqahtani, A. H., ... & Amin, Y. (2023). A High Performance All-Textile Wearable Antenna for Wristband Application. *Micromachines*, *14*(6), 1169. https://doi.org/10.3390/mi14061169

[4] Sohail, A. (2023). Genetic algorithms in the fields of artificial intelligence and data sciences. Annals of Data *Science*, *10*(4), 1007-1018. https://doi.org/10.1007/s40745-021-00354-9

[5] Song, Y., Cai, X., Zhou, X., Zhang, B., Chen, H., Li, Y., ... & Deng, W. (2023). Dynamic hybrid mechanism-based differential evolution algorithm and its application. *Expert Systems with Applications*, *213*, 118834. https://doi.org/10.1016/j.eswa.2022.118834

[6] Nayak, J., Swapnarekha, H., Naik, B., Dhiman, G., & Vimal, S. (2023). 25 years of particle swarm optimization: Flourishing voyage of two decades. *Archives of Computational Methods in Engineering*, *30*(3), 1663-1725. https://doi.org/10.1007/s11831-022-09849-x

[7] Kuznetsov, A., Frontoni, E., Romeo, L., Poluyanenko, N., Kandiy, S., Kuznetsova, K., & Beňová, E. (2023). Optimizing Hill Climbing Algorithm for S-Boxes Generation. *Electronics*, *12*(10), 2338. https://doi.org/10.3390/electronics12102338

[8] Rathi, N., Chakraborty, I., Kosta, A., Sengupta, A., Ankit, A., Panda, P., & Roy, K. (2023). Exploring neuromorphic computing based on spiking neural networks: Algorithms to hardware. *ACM Computing Surveys*, *55*(12), 1-49. https://doi.org/10.1145/3571155

[9] Yue, Y., Cao, L., Lu, D., Hu, Z., Xu, M., Wang, S., ... & Ding, H. (2023). Review and empirical analysis of sparrow search algorithm. *Artificial Intelligence Review*, 1-53. https://doi.org/10.1007/s10462-023-10435-1

[10] Yu, M., Xia, B., Gao, Y., & Zhang, L. (2023). CSO Cooperative Localization Algorithm in UWB Sensor Network. *Wireless Personal Communications*, *130*(1), 579-592. https://doi.org/10.1007/s11277-023-10299-2

[11] Gen, M. & Lin, L. (2023). *Genetic algorithms and their applications. Springer handbook of engineering statistics*. London: Springer London, 635-674. https://doi.org/10.1007/978-1-4471-7503-2_33

[12] Xue, Z., Yao, S., Ma, H., Zhang, C., Zhang, K., & Chen, Z. (2023). Thermo-economic optimization of an enhanced geothermal system (EGS) based on machine learning and differential evolution algorithms. *Fuel*, *340*, 127569. https://doi.org/10.1016/j.fuel.2023.127569

[13] Zheng, L., Yu, W., Li, G., Qin, G., & Luo, Y. (2023). Particle Swarm Algorithm Path-Planning Method for Mobile Robots Based on Artificial Potential Fields. *Sensors*, *23*(13), 6082. https://doi.org/10.3390/s23136082

[14] Tu, Q. (2023). *MPC Based Car-Following Control Considering Uphill and Downhill (No. 2023-01-0691)*. SAE Technical Paper. https://doi.org/10.4271/2023-01-0691

[15] Malekshah, E. H., Abed, A. M., & Aybar, H. Ş. (2023). Thermal analysis of multi-finned plate employing lattice Boltzmann method based on Taylor-series/least-squares. *Engineering Analysis with Boundary Elements*, *146*, 407-417. https://doi.org/10.1016/j.enganabound.2022.11.008

[16] Kurani, A., Doshi, P., Vakharia, A., & Shah, M. (2023). A comprehensive comparative study of artificial neural network (ANN) and support vector machines (SVM) on stock forecasting. *Annals of Data Science*, *10*(1), 183-208. https://doi.org/10.1007/s40745-021-00344-x

[17] Murugan, R. A. & Sathyabama, B. (2023). Night Vision Object Tracking System Using Correlation Aware LSTM-

Based Modified Yolo Algorithm. *Intelligent Automation and Soft Computing*, *36*(1), 353-368. https://doi.org/10.32604/iasc.2023.032355

[18] Ni, Z., Fan, Y., Hang, Z., Zhu, F., Wang, Y., Feng, C., & Yang, J. (2023). Damped vibration analysis of graphene nanoplatelet reinforced dielectric membrane using Taylor series expansion and differential quadrature methods. *Thin-Walled Structures*, *184*, 110493. https://doi.org/10.1016/j.tws.2022.110493

[19] Agiza, H. N., Sohaly, M. A., & Elfouly, M. A. (2023). Small two-delay differential equations for Parkinson's disease models using Taylor series transform. *Indian Journal of Physics*, *97*(1), 39-46. https://doi.org/10.1007/s12648-021-02263-2

[20] Qu, Z., Li, Y., Jiang, X., & Niu, C. (2023). An innovative ensemble model based on multiple neural networks and a novel heuristic optimization algorithm for COVID-19 forecasting. *Expert Systems with Applications*, *212*, 118746. https://doi.org/10.1016/j.eswa.2022.118746

[21] Wang, W. C., Xu, L., Chau, K. W., Liu, C. J., Ma, Q., & Xu, D. M. (2023). Cε-LDE: A lightweight variant of differential evolution algorithm with combined ε constrained method and Lévy flight for constrained optimization problems. *Expert Systems with Applications*, *211*, 118644. https://doi.org/10.1016/j.eswa.2022.118644

[22] Zhang, X., Zhong, C., & Abualigah, L. (2023). Foreign exchange forecasting and portfolio optimization strategy based on hybrid-molecular differential evolution algorithms. *Soft Computing*, *27*(7), 3921-3939. https://doi.org/10.1007/s00500-022-07526-6

[23] Narayan, V., Daniel, A. K., & Chaturvedi, P. (2023). E-FEERP: Enhanced Fuzzy based Energy Efficient Routing Protocol for Wireless Sensor Network. *Wireless Personal Communications*, 1-28. https://doi.org/10.1007/s11277-023-10434-z

[24] Jain, D., Shukla, P. K., & Varma, S. (2023). Energy efficient architecture for mitigating the hot-spot problem in wireless sensor networks. *Journal of Ambient Intelligence and Humanized Computing*, *14*(8), 10587-10604. https://doi.org/10.1007/s12652-022-03711-5

[25] Hongfan, G. & Zhangyan, Z. (2023). Research on obstacle climbing gait structure design and gait control of hexapod wall climbing robot based on STM32F103 core controller. *Mechanics & Industry*, *24*, 20. https://doi.org/10.1051/meca/2023019

[26] Saban, M., Bekkour, M., Amdaouch, I., El Gueri, J., Ait Ahmed, B., Chaari, M. Z., & Aghzout, O. (2023). A Smart Agricultural System Based on PLC and a Cloud Computing Web Application Using LoRa and LoRaWan. *Sensors*, *23*(5), 2725. https://doi.org/10.3390/s23052725

[27] Jiang, W., Liu, T., Chen, H., Song, C., Chen, Q., & Geng, T. (2023). Multi-frequency phase observable-specific signal bias estimation and its application in the precise point positioning with ambiguity resolution. *GPS Solutions*, *27*(1), 4.https://doi.org/10.1007/s10291-022-01325-0

[28] Aguila-Leon, J., Vargas-Salgado, C., Chiñas-Palacios, C., & Díaz-Bello, D. (2023). Solar photovoltaic Maximum Power Point Tracking controller optimization using Grey Wolf Optimizer: A performance comparison between bio-inspired and traditional algorithms. *Expert Systems with Applications*, *211*, 118700. https://doi.org/10.1016/j.eswa.2022.118700

[29] Ali, S., Prado, A., & Pervaiz, M. (2023). Hybrid backstepping-super twisting algorithm for robust speed control of a three-phase induction motor. *Electronics*, *12*(3), 681. https://doi.org/10.3390/electronics12030681

[30] Zhang, D., Shen, S., Wu, J., Wang, F., & Han, X. (2023). Kinematic trajectory accuracy reliability analysis for industrial robots considering intercorrelations among multi-point positioning errors. *Reliability Engineering & System Safety*, *229*, 108808. https://doi.org/10.1016/j.ress.2022.108808

Contact information:

Wei LI
(Corresponding author)
School of Electronic Information Engineering,
Geely University of China,
Chengdu, 641423
E-mail: li.wei.77@163.com

Xeu-qin MENG
School of Electronic Information Engineering,
Geely University of China,
Chengdu, 641423

Chang-song MA
School of Electronic Information Engineering,
Geely University of China,
Chengdu, 641423